Phase structure and fracture toughness of the polyethersulfone-modified bismaleimide resin

Phase structure and fracture toughness of the polyethersulfone-modified bismaleimide resin

X G Li[1], W Q Mu[1], Y T Li[1, 2], H H Qian[1,2,*], L J Cheng[1, 2] and J L Liu[1, 2]

[1] AECC Beijing Institute of Aeronautical Materials, Beijing, 100095, China
[2] Aviation Key Laboratory of Science and Technology on Materials and Application Research for Vibration and Noise Reduction, AECC Beijing Institute of Aeronautical Materials, Beijing, 100095, China

*E-mail: huanghai.qian@biam.ac.cn

Abstract. Although bismaleimide (BMI) resins have been widely used for aerospace applications, owing to their good thermal stability, humidity resistance and excellent mechanical property, they are usually brittle due to high crosslinking density and vulnerable to cracking. Hence enhancement in fracture toughness is desired. Polyethersulfone (PES) is a kind of high-performance thermoplastic materials. The blends of PES and BMI were initially homogeneous solutions but become separated in phases during the polymerization of a thermoset. The morphologies of the BMI/PES resin system were studied. The effect of phase structure on the final mechanical properties was investigated

1. Introduction

Bismaleimide (BMI) resins are considered as a kind of high-performance thermoset materials for the matrix in advance composites, due to their good thermal stability, excellent corrosion resistance and humidity resistance, and good retention of mechanical properties at high temperatures [1]. However, bismaleimide resins suffer from brittleness owing to a highly crosslinked structure. To improve the fracture toughness of BMI, several approaches have been developed [2]. One approach is to use various thermoplastic to modify the fracture toughness properties of BMI. These thermoplastics included PESF [3], PEI [4], poly (phthalazinone ether ketone) [5], PEEK [6], polyimide [7] and poly (arylene ether) [8].

In most cases, the thermoplastic is initially dissolved in the thermoset prepolymer, developing a homogeneous solution. And then a phase separation occurs in the blend of thermoplastic and thermoset resin during the polymerization of a thermoset. This process is known as polymerization-induced phase separation [9,10]. The final properties of the thermoplastic/thermoset blend are primarily determined by the developed phase structures [11-14].

This paper will present the BMI/PES blends by investigating the morphologies and furthermore the relationship between morphologies and the mechanical properties was discussed in detail.

2. Experimental

2.1. Materials

The BMI used a combination of N, N'-4, 4'-bismaleimdodiphenylmethane (BDM), 0, 0'-diallyl-bisphenol A (DABPA), and phenol. It is an RTM-able BMIs developed by the National Key Laboratory of Advanced Composites, with the trademark of BMI 6421. Polyethersulfone (PES), employed as

toughener in this study was hydroxyl-terminated polyether sulfone Virantage® VW-10200 RFP, supplied by Solvay Specialty Polymers [15]. All materials were commercial products and were used as received without further purification. Figure 1 shows the molecular structure of the BDM, DABPA, and PES, respectively.

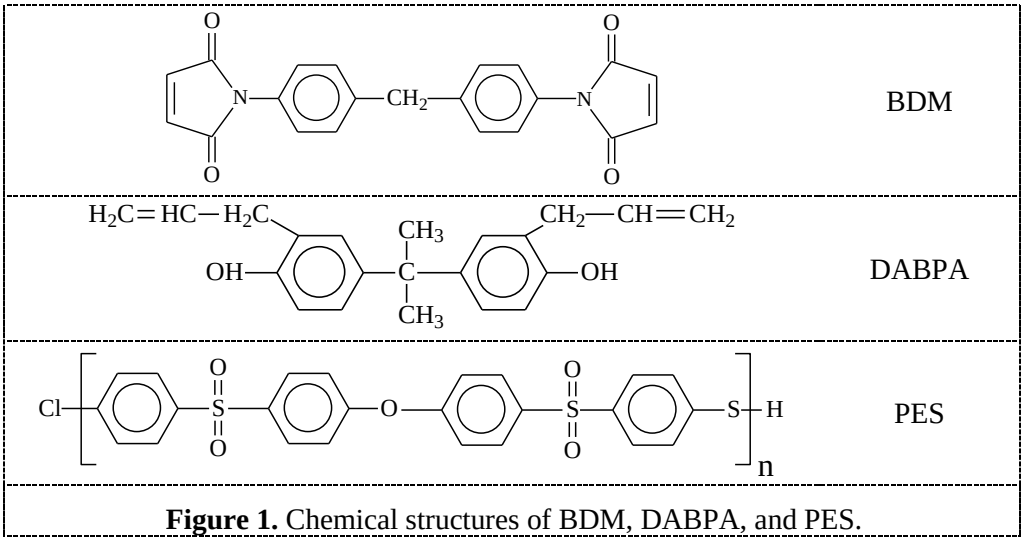

Figure 1. Chemical structures of BDM, DABPA, and PES.

2.2. Sample preparation

BMI/PES blends were prepared as follows. PES was dissolved in the mixture of DABPA and phenol at 120 ℃, then BDM was added to the blend at 130 ℃. The mixture was mechanically stirred continuously at 130 ℃ for 0.5 h until an optically clear and transparent blend was obtained, then cured under full vacuum for 30 min to remove any bubbles. After curing, the sample was allowed to cool slowly to room temperature. Table 1 demonstrates the composition of uncrosslinked blends of BMI/PES. Figure 2 gives the curing profile of BMI/PES blends.

Table 1. Designation of the blends of BMI and PES

Sample name	BMI (phr)	PES (phr)
BMI/PES-0	100	0
BMI/PES-5	100	5
BMI/PES-10	100	10
BMI/PES-15	100	15
BMI/PES-20	100	20
BMI/PES-25	100	25

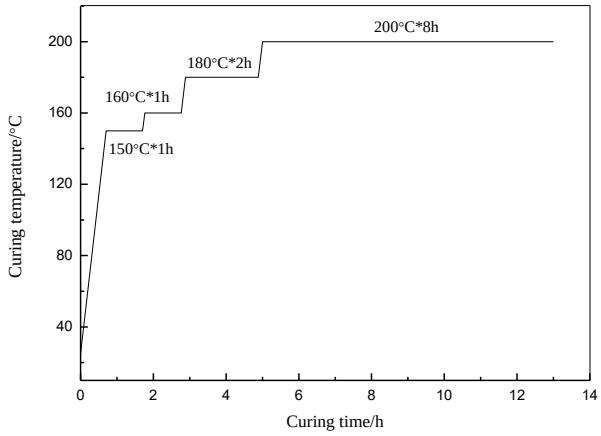

Figure 2. The curing profile of BMI/PES blends.

2.3. Measurements

2.3.1. Scanning electron microscope (SEM). The morphology of the cured resins was examined by SEM, using a Hitachi S-4800. The samples were fractured in liquid nitrogen, coated with a layer of gold and then observed by SEM.

2.3.2. Fracture toughness tests. Fracture toughness test was made using Single-Edge Notched Bending (SENB) geometry in three-point bending, following the ASTM D5045 Standard [16]. Figure 3 shows the adopted sample geometry.

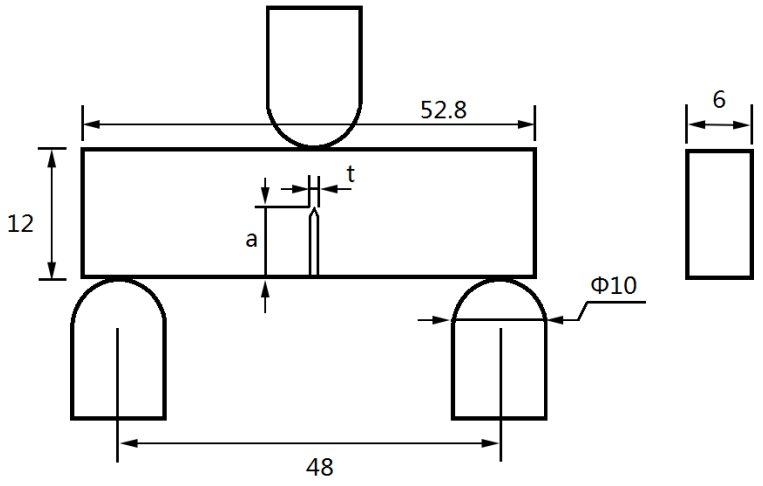

Figure 3. Dimensions of the SENB specimen.

Samples were cut from the cast resin plate with nominal dimensions of 52.8×12×6 mm. A 4.5 mm deep notch was machined by a diamond saw, and a fresh razor blade was lightly tapped into the tip of the notch by a hammer to create a natural pre-crack. The pre-cracked SENB specimens were loaded under three-point bending using a universal testing machine (Instron 3345) at a rate of 0.5 mm/min. Figure 4 shows an example of BMI/PES sample with the produced notch geometry.

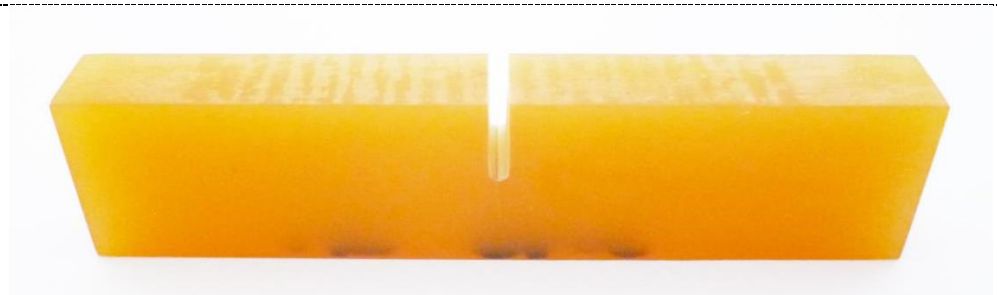

Figure 4. Dimensions of the single edge notched resin specimen.

Five samples were tested in each category. Failure load from each test was recorded. The values of K_{IC} and G_{IC}, respectively, the critical stress intensity factor also known as the critical plane strain fracture toughness and the critical strain energy release rate were calculated from the experimental curves.

The tentative value of fracture toughness, K_Q, is determined by Eq. (1):

$$K_Q = f(x)\left(\frac{P_Q}{BW^{1/2}}\right), \mathrm{W} = 2\mathrm{B}, x = \frac{a}{W} \quad (1)$$

where B is specimen thickness, W is specimen width, a is crack length.
with

$$f(x) = 6x^{1/2}\frac{[1.99 - x(1-x)(2.15 - 3.93x + 2.7x^2)]}{(1+2x)(1-x)^{3/2}} \quad (2)$$

The resulting K_Q is accepted as a valid critical stress intensity factor value K_{IC} if all characteristic lengths of the samples (X=B, a or the ligament (W-a) comply with the condition:

$$B, a, W - a \geq 2.5\left(\frac{K_Q}{\sigma_{YS}}\right)^2 \quad (3)$$

Then, GIC can be determined by equation 4:

$$G_{IC} = \frac{1-\nu^2}{E}K_{IC}^2 \quad (4)$$

where v represents Poisson's ratio and E is Young moduli.

The value of the yield stress (σ_{YS}), v and E required for the toughness calculations can be measured using cast dog-bone specimens tested in tension using ASTM standards D638.

3. Results and discussion

3.1. Morphology

Figure 5 shows the morphologies of BMI/PES resin system by SEM micrographs. The SEMs are shown at different magnifications for better observation.

The BMI resin systems without modifier exhibited a single phase morphology with a brittle fracture surface (figure 5a). Contrarily, all resin systems modified with PES showed heterophasic morphologies, indicating that a phase separated in these materials.

There were three different types of phase morphologies showed in the PES modified BMI resins: sea-island structure, co-continuous structure, and phase-inverted structure. The type of morphology varied with the loading of thermoplastic PES modifier in the blend.

The BMI/PES-5 resin system generated the sea-island morphology with PES-rich particles dispersed in a BMI-rich matrix (figure 5b). The size of spherical particles was in the range of 5-8 μm.

BMI/PES-15, BMI/PES-20, and BMI/PES-25 showed the phase-inverted morphology, which also called the phase-inverted nodular structure (figures 5f, 5g and figure 5h). This nodular morphology consisted of particles BMI-rich dispersed in a continuous PES-rich matrix. An increase in the loading of PES led to an increase in the loading of dispersed particles and a decrease in their average size(5–20μm). This trend can be ascribed to the increase in viscosity of the medium of BMI/PES blend with the amount of PES increasing. This hinders the diffusion of matter and favors nucleation, resulting in more dispersed particles but smaller size. The micrographs clearly showed the excellent interfacial bonding between BMI and PES with few bared BMI-rich particles.

The co-continuous morphology (figure 5d and figure 5f) was developed by BMI/PES-10. BMI/PES-10 also contained a complex morphology with sea-island morphology and phase-inverted structure irregularly generated in the resin.

A feature observed in some of the morphologies was a second phase separation structure (figure 5c).The second phase separation can be described as follow: the PES-rich phase after phase separation contains a vast number of low molecular weight monomers and oligomers of DABPA-BDM. As for curing of DABPA-BDM component proceeds, the PES-rich phase comes to be immiscible with the dissolved BMI component and eventually separating the BMI-rich domains.

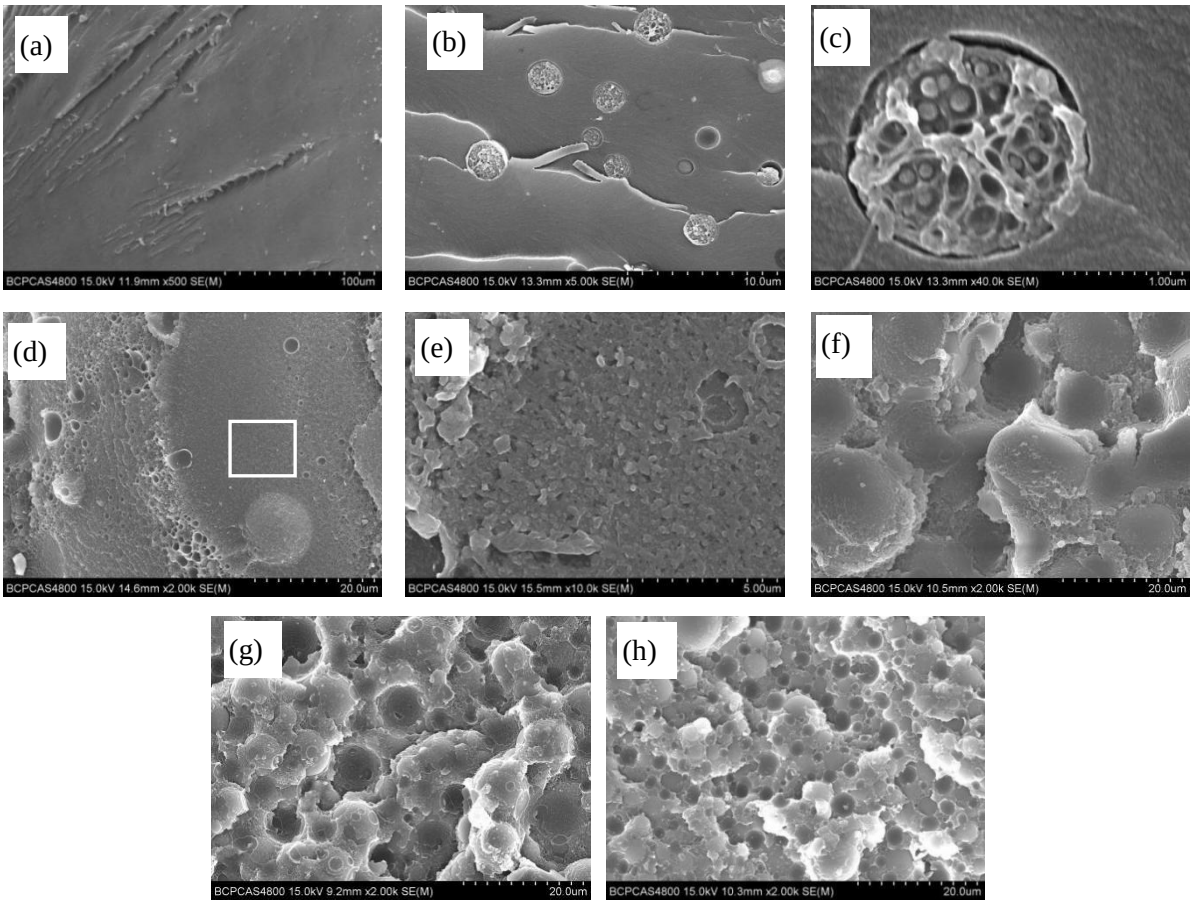

Figure 5. SEM of the morphologies of the BMI/PES resin system.
(a) BMI/PES-0; (b) BMI/PES-5 ; (c) high magnifications of BMI/PES-5; (d)BMI/PES-10; (e) high magnifications of BMI/PES-10; (f)BMI/PES-15; (g) BMI/PES-20; (h)BMI/PES-25.

3.2. Mechanical properties

Figure 6 shows the typical SENB curves of BMI/PES resin. The BMI resin systems without modifier showed unstable crack propagation. The load dropped suddenly, and the structural failure occurred quickly. It is worth to note that the BMI resin toughened with PES shows more non-linear load decrease after the maximum load than the neat BMI resin, indicating a gentle crack propagation. BMI/PES-15 exhibited the highest peak load.

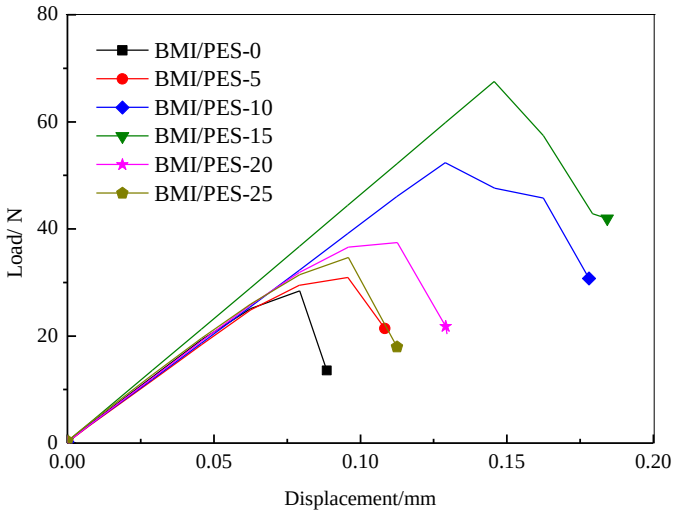

Figure 6. Typical load-displacement of BMI/PES resin under SENB tests.

The fracture toughness of BMI/PES resin characterized by K_{IC} and G_{IC} are given in figure 7. The modifier PES improved the fracture toughness of BMI matrix substantially. The fracture toughness approximately linear increased with the incorporation of PES, attained its maximum, and then was gradually decreased. The BMI/PES resin showed maximum fracture toughness at 15 phr. K_{IC} increased up to 1.22 MPa•m$^{1/2}$ from 0.53 MPa•m$^{1/2}$ of neat resin while G_{IC} increased from 58 up to 257 J•m^{-2}. This significant improvements of fracture toughness due to the incorporation of PES can be ascribed to the phase separated and inverted structure. Tougher resin increases the plastic yielding zone size ahead of the crack tip, giving greater load redistribution away from the crack tip as well as more crack-tip blunting through interfacial debonding of the BMI-rich particles phases along with a plastic drawing of the PES-rich phases and hence more energy absorption.

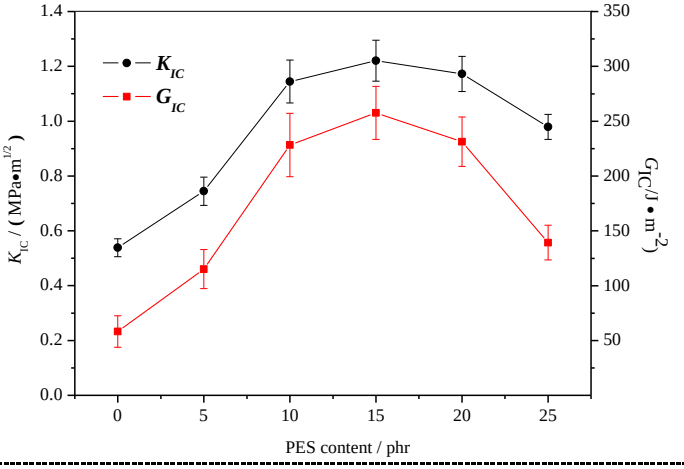

Figure 7. Fracture toughness of BMI/PES resin.

4. Conclusions

The morphology generated in the blend resin based on a polyethersulfone (PES) modifier and BDM/DABPA systems, were observed.

Three different types of morphologies were gained determined by the initial concentration of PES: sea-island morphology of PES-rich particles surrounded with the continuous BMI-rich phase for low PES content (PES 5phr), nodular morphology of BMI-rich particles surrounded with the continuous PES-rich phase for high PES content (PES 15, 20, and 25phr), and co-continuous morphology for intermediate PES content (PES 10phr). An increase in the loading of PES resulted in a decrease in the average size of BMI-rich particles (5–20μm) and an increase in their loading in the nodular morphology.

The fracture toughness increased with the incorporation of PES attaining the maximum then gradually decreases. Compared to neat BMI resin, K_{IC} of BMI/PES-15phr increased by about 130% while G_{IC} of BMI/PES-15phr improved by about 343%. This can be attributed to the phase separated and inverted structure of BMI/PES system. During crack growth, the particle phase acted as stress concentrator, which resulted in plastic yield and drawing of the continuous PES phase, deflecting the fracture path, and hence increasing energy absorption.

Acknowledgments

Authors wish to acknowledge the assistance of Dr. Dong H.M. at AECC Beijing Institute of Aeronautical Materials for the technical support.

References

[1] Dong H M, An X F, Yi X S, Yan L, Su Z T and Bao J W 2015 *J. Mater. Eng.* **43** 89-100.
[2] Dong H M, Yi X S, An X F, Zhang C Q, Yan L and Deng H 2014 *Acta Material Compositae Sinica* **31** 273-285
[3] Liu X, Yu Y and Li S 2006 *Eur. Polym. J.* **42** 835-842
[4] Zhao L, Li L, Tian J X and Zhuang J H 2004 *Compos Part A-Appl S* **35** 1217-1224
[5] Han Y, Liao G, Xu Y, Yu G and Jian X 2009 *Polym. Eng. Sci.* **49** 2301–2308
[6] Chu P P, Wu C S, Liu P C, Wang T H and Pan J P 2010 *Polymer* **51** 1386-1394
[7] Pascal T, Mercier R, Sillion B 1989 *Polymer* **30** 739-744
[8] Stenzenberger H D, König P 1993 *High Perform. Polym.* **5** 123-137
[9] Kim J Y, Cho C H, Palffy-Muhoray P and Kyu T 1993 *Phys. Rev. Lett.* **71** 2232-2235
[10] Luo K 2006 *Eur. Polym. J.* **42** 1499-1505
[11] López J, Ramírez C, Abad M J, Barral L, Cano J and Díez F J 2010 *J. Appl. Polym. Sci.* **85** 1277-1286
[12] Zucchi I A, Galante M J, Williams R J J 2005 Polymer **46** 2603-2609
[13] Prolongo M G, Arribas C, Salom C and Masegosa R M 2007 *J. Therm. Anal. Calorim.* **87** 33-39
[14] Rico M, López J, Montero B and Bellas R 2012 *Eur. Polym. J.* **48** 1660-1673
[15] Zhang C Q, An X F, Dong H M, Yan L and Gao J P 2012 *China Thermosetting Resin* 33-36
[16] Sham Prasad M S, Venkatesha C S, Jayaraju T 2011 *J. Miner. Mater.Charact.Eng* **10** 1263-1275